Composite materials with combined electronic and ionic properties

Noam Ralbag[a], Meirav Mann-Lahav[b], Elena S. Davydova[b,c], Uri Ash[b], Reuven Galed[b], Michael Handl[d], Renate Hiesgen[d], Emanuele Magliocca[e], William Mustain[e], Jin He[a], Peixi Cong [f,g], Andrew Beale[f,g], Gideon S. Grader[b,c,*], David Avnir[a,*] and D. R. Dekel[b,c,*]

[a] Institute of Chemistry and the Center for Nanoscience and Nanotechnology, The Hebrew University of Jerusalem, Jerusalem 9190402, Israel

[b] The Wolfson Department of Chemical Engineering, Technion−Israel Institute of Technology, Haifa 3200003, Israel

[c] The Nancy & Stephan Grand Technion Energy Program (GTEP), Technion−Israel Institute of Technology, Haifa 3200003, Israel

[d] Hochschule Esslingen - University of Applied Sciences, 73728 Esslingen, Germany

[e] Department of Chemical Engineering, University of South Carolina, USA

[f] Department of Chemistry, University College of London, Gordon Street, London, WC1H 0AJ, UK

[g] Research Complex at Harwell, Rutherford Appleton Laboratory, Didcot, OX110FA, UK

*Correspondence: G.S.G.: grader@technion.ac.il; D.A.: David.Avnir@mail.huji.ac.il; D.R.D: dario@technion.ac.il

Summary

In this work we develop a new type of composite material that combines both electrocatalytic and ionic properties, by doping silver metal catalyst with an anion conducting ionomer at the molecular level. We show that ionomer entrapment into the silver metallic structure is possible, imparting unique properties to the catalytic character of the metallic silver. The novel composite material is tested as the cathode electrode of fuel cells, showing significant improvement in cell performance, as compared to the undoped counterpart. This new type of materials may then replace the current design of electrodes in advanced fuel cells or other electrochemical devices. The possibility to merge different properties into one composite material by molecular entrapment in metals can open the way to new materials leading to unexplored fields and applications.

1. Introduction

Electrical conductivity is one of the main properties of metals and one of the most important material properties in research and industry. Ionic conductivity, on the other hand, can be found in other types of materials, mainly ion conducting polymers, some ceramic materials, and ionic liquids. The possibility to merge these properties into one composite material can open the way to new applications. Such a possibility has been advanced by a recent materials methodology which enables the entrapment of polymers, small molecules, enzymes and nanoparticles within metals[1,2]. This new type of materials, denoted dopant@metal[3,4,13,14,5–12] has properties that are a combination, sometimes synergetic, of the properties of the two components. Various methods for the molecular entrapment have been developed, mainly based on reducing the metal cation in the presence of the species to be entrapped within the metal. Metals which have been doped so far include silver, gold, copper, iron, gallium[4], palladium, platinum, and several alloys[11,12,15]. This materials' methodology already proved useful in a number of applications, including catalysis, antibacterial materials, batteries, and in alteration of metal properties, as the work function[16] and corrosion resistance[17]. The dopants are physically entrapped within the narrow pores and cages of agglomerated metallic nanocrystals, a few nanometers in size. The interstitial porosity of the composite material enables reactions with the dopants, as well as in-diffusion of substrate molecules to the (active) dopant and out-diffusion of product molecules. Entrapment is a distinctly different process compared to adsorption: Adsorption involves 2D arrangement where the molecules interact with the metallic surface metal typically with one moiety and are typically easily washed away, while entrapment is a 3D process, in which all portions of the molecule interact with the walls of the metallic cage, and their extraction requires special conditions. Of relevance to this study are the reports on successful entrapment within metals of polymers[17–19] including the catalytically active Nafion@Pd[20], Nafion@Ag and PVBA@Ag[21], which exhibit also ion exchange ability, as well as the reports on the electrocatalytic activity of doped Pd[9] or Cu[10].

In this work, we extend the concept of molecular-level doping of metals, and develop a material with electrocatalytic activity that combines both ionic and electronic conductivities. This type of materials may replace the current design of electrocatalysts, ionomers and/or electrodes for advanced fuel cells or other electrochemical devices.

Specifically, as first part of our study, we entrap an anion conducting ionomeric material[22,23] within metallic silver, which is a well-known electrocatalyst for oxygen reduction reactions in alkaline medium[24]. The new type of material is then tested in an anion-exchange membrane fuel cell device, proving its successful performance.

2. Experimental details

Material preparation:

Entrapment of FAA-3 in silver (FAA-3@Ag): The following procedure was used for the entrapment of FAA-3 conducting ionomer into metallic silver – 240 mg of the ionomer FAA-3 bromide was dissolved in 3 mL of methanol under continuous stirring. $AgNO_3$; 3.04 g (17.9 mmol) was dissolved in 20 mL of triple distilled water in a 15 °C water bath. After 10 min of stirring, 950 mg (10.4 mmol) of $NaH_2PO_2 \times \sim 0.2\ H_2O$ and the dissolved ionomer were added to the $AgNO_3$ solution. The solution was kept under stirring and cooling for 24 hours and then filtered under vacuum, using mixed cellulose esters filter paper (pore size 0.22 μm). The dark-grey powder was dried under vacuum overnight and then collected, yielding ~2.1 g. In order to prepare rectangular chips of the composite, around 120 mg of the powder was placed in a $5 \times 10\ mm^2$ press mold and pressed under vacuum at 4000 psi for 10 min.

Pure Ag and adsorbed FAA-3: For comparative purposes, pure Ag powder was synthesized by the same method but without the addition of the ionomer. Also, for comparative purposes of 3D entrapment *vs.* 2D adsorption two adsorption methods were applied: (1) Adsorption from Solution - 50 mg of the pure Ag powder was dispersed in 2 mL of triple distilled water and kept under stirring. After 10 min, 12 mg of the ionomer in 150 μL methanol was added. The solution was kept at 15 °C under stirring for 24 hours and then the product was filtered and dried as described above. (2) Evaporative coating - 58 mg of the ionomer was dissolved in 10 mL of methanol. After 10 min, 800 mg of the pure Ag powder was added to the solution. The combined dispersion was stirred for 1 hour and then placed in an oven at 85 °C for 24 hours to evaporate the solvent. The resulting solid were crushed and homogenized with mortar and pestle.

Material characterization:

Ion exchange capacity (IEC) measurements: A general procedure to measure IEC was followed[25,26]: The bromide of the entrapped FAA-3 was anion-exchanged to hydroxide form by soaking the powder in 10 mL of 1 M NaOH solution for 48 hours. The composite was then filtered and dried under vacuum. Then ~110 mg of powder or pressed pellet was placed in a glass vial and then 15 mL of 0.01 M HCl was added while stirring for 72 hours. The samples were then back-titrated with 0.01 M NaOH solution using Boeco DCB 2500 digital burette (±0.2 vol%) and HANNA instruments HI2020 pH-meter (±0.001 pH). The IEC (mmol g^{-1}) is calculated using equation 1[27]

Equation 1 $$\boldsymbol{IEC} = \frac{\boldsymbol{n_i}(\mathbf{H^+}) - \boldsymbol{n_f}(\mathbf{H^+})}{\boldsymbol{m}\,(\mathbf{composite})},$$

where n_i and n_f are the number of free hydronium ions in the control and composite titrations, respectively.

Water uptake (WU) measurements: The WU was measured using a VTI SA+ instrument (TA Instruments, USA). The RH was determined with a two-stage chilled-mirror dew-point analyzer and adjusted by mixing dry and humidified nitrogen gas. Each sample was initially dried in situ for 60-90 min at 70 °C and RH ~0% till equilibration. Afterwards, RH was step-changed in intervals of 10%, 30%, and 50%. Each RH step was maintained until the sample weight reached equilibrium (<0.001 wt% change in 5 min). WU is calculated from the "wet" weight (W_{wet}) at each equilibrium and the "dry" weight (W_{dry}) at the end of the initial drying step, according to[28]

Equation 2 $$\mathbf{WU} = \frac{\boldsymbol{W}\mathbf{wet} - \boldsymbol{W}\mathbf{dry}}{\boldsymbol{W}\mathbf{dry}} \times \mathbf{100}\%$$

Performance:

Catalytic activity measurements: Floating gas diffusion electrode (GDE) method[29] was used to measure catalytic activity towards oxygen reduction reaction (ORR) of the materials. Working electrodes were prepared as described elsewhere[30] by pressing Ni mesh (woven 100 mesh, wire diam. 0.1 mm, Alfa Aesar) with 500 ± 20 µm-thick gas diffusion layer (GDL), comprising 35 wt% polytetrafluoroethylene (PTFE, 60 wt% dispersion in H_2O, Sigma Aldrich) and 65 wt% carbon black VXCMAX22 (Table S1,

Cabot, USA). The catalyst powder was applied on the GDL resulting in three-layered gas diffusion electrodes with the geometric surface area of 1 cm^2. Electrodes were pressed twice under ca. 400 kg cm^{-2} for 2 min at room temperature: first, to assemble Ni mesh and GDL, and then to embed applied catalytic layer into the GDL. All the electrochemical measurements were carried out in three-electrode glass water-jacketed electrochemical cell in 1 M KOH at 60 °C. Pt wire in separated glass-fritted compartment served as the counter electrode. Mercury-mercury oxide (Hg/HgO) electrode in 1 M KOH was utilized as the reference electrode. O_2 (99.999%, Maxima, Israel) was purged above the floating GDE during the measurements of the catalytic activity in ORR. The polarization curves of ORR were recorded with the potential sweep rate of 1 mV s^{-1}.

Anion-exchange membrane fuel cell tests: AEMFC test procedures followed the general protocols used in our previous work[31–34] unless it is indicated differently. The membrane used in this work was a LDPE-g-poly(-VBTMA+Cl-) AEM[35]. Prior to the fuel cell assembly, the GDEs and AEMs were separately immersed in aqueous KOH (1 M, Fisher Chemical, pellets/certified ACS) for 60 min, replacing the solution every 20 min to ensure complete ion-exchange. During this hydration and ion-exchange process, no substantial electrocatalyst or (anion exchange ionomer) AEI particles were observed to wash off the GDE surface, showing adequate adhesion of the catalyst layers onto the GDLs. Excess aqueous KOH and water were removed from the electrodes and membrane with a laboratory cloth prior to assembly, in order to avoid carbonation process during the fuel cell tests[36–39]. Each set of GDEs and AEM were pressed together in-cell to form the AEMFC with no prior hot pressing. The cell were secured in 5 cm^2 Fuel Cell Technologies hardware between two single pass serpentine flow graphite plates using 150 µm PTFE gaskets with 20% pinch (4.5 N m torque). An 850e Scribner Fuel Cell Test Station was used for all testing. H_2 and O_2 gas feeds (~1 atm absolute) were supplied to the anode and cathode, respectively. The dew point of the H_2 fed to the anode was 79 °C, and the dew point of the O_2 fed to the cathode was 79 °C. The cell temperature was 80 °C ± 0.5 °C. All of the polarization curves shown were collected under potentiometric control at a scan rate of 10 mV s^{-1}.

Additional experimental details in the Supplementary Material: Chemicals, microscopy methods, preparation of the anion-exchange membrane electrode assembly (MEA), various additional instrumentations.

3. Results and discussion

Material characterization of FAA-3@Ag composite and proofs of entrapment

To achieve a dual functionality of both electric conductivity and ionic conductivity in one composite material aimed at functioning as an anion-exchange membrane fuel cell (AEMFC) cathode, entrapment of FAA-3 polymer into the particles of Ag was carried out. The selection of metallic Ag as the entrapment matrix for ion conductive polymer is due to its relatively high catalytic activity in oxygen reduction reaction (ORR)[40]. The feasibility of Ag as the AEMFC cathode material was successfully demonstrated in[31–33]. Aromatic ionomer FAA-3 is a widely used ion-conducting material in fuel cells[41]. Although its stability at low hydration environment is questionable,[42,43] this ionomer was selected for this initial work due to its good stability in liquid water[44], and its relatively high ion exchange capacity (IEC)[22,45] (2.4−2.9 mmol g^{-1}).

The main challenge in the entrapment of this ionomer is its insolubility in water which is the preferred solvent for the entrapping-reduction reaction of the metallic cation[18,21]. Search for suitable new entrapment conditions led to the procedure of pre-dissolving of the polymer in methanol along with delicate control of reaction conditions, which enabled the entrapment before polymer phase-out from the water-methanol solution. The resulting product is a composite metallic powder, the microstructure of which is hierarchical (**Error! Reference source not found.**) – it is composed of clusters in the tens μm range; these clusters are composed of metal aggregates in the size range of 0.1−1 μm, which in turn are composed of nanometric silver crystallites (~57 nm, determined from the XRD pattern **Error! Reference source not found.**). The crystallites size of pure Ag prepared by the same method are twice as large - ~119 nm. The size reduction of the silver nanocrystallites during the entrapment process is due to the adsorptive masking effect of the polymer of the growing crystallite. This microstructure leads to a nitrogen-BET surface area of 2.25 m^2 g^{-1} displaying an adsorption-desorption isotherm which is

typical of interstitial porosity (Figure S1, Supplementary Material), to Barrett, Joyner and Halenda (BJH) average mesopore diameter of 63.9 nm and BJH pore volume of 0.028 $cm^3\ g^{-1}$. (For pure Ag, the surface area is 0.13 $m^2\ g^{-1}$ and the BJH average pore diameter is 47.5 nm).

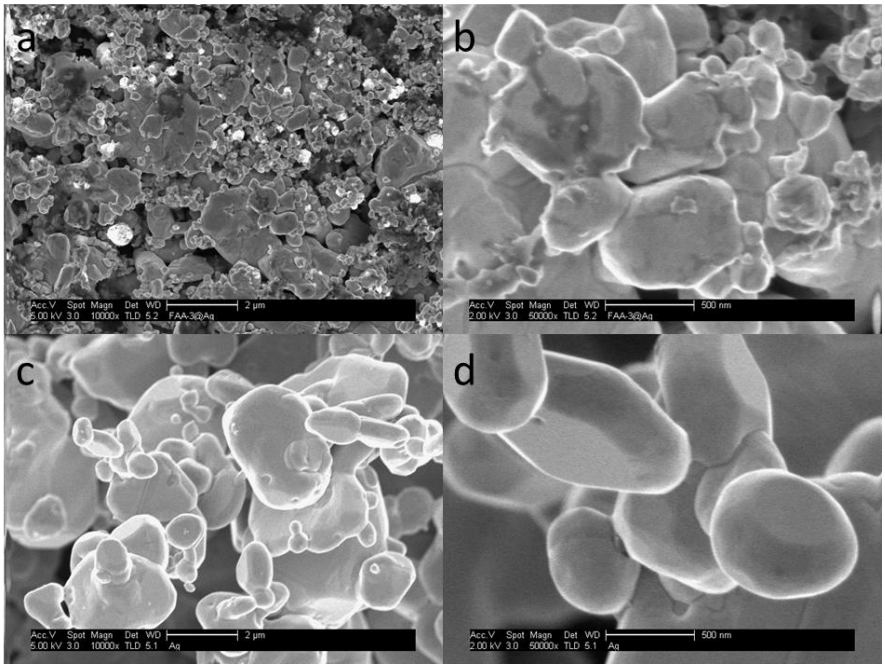

Figure 1: High resolution SEM (HR-SEM) images of FAA-3@Ag (a - bar: 2 µm, b – bar: 500 nm) compared to pure Ag (c – bar: 2 µm, d – bar: 500 nm) prepared by the same method

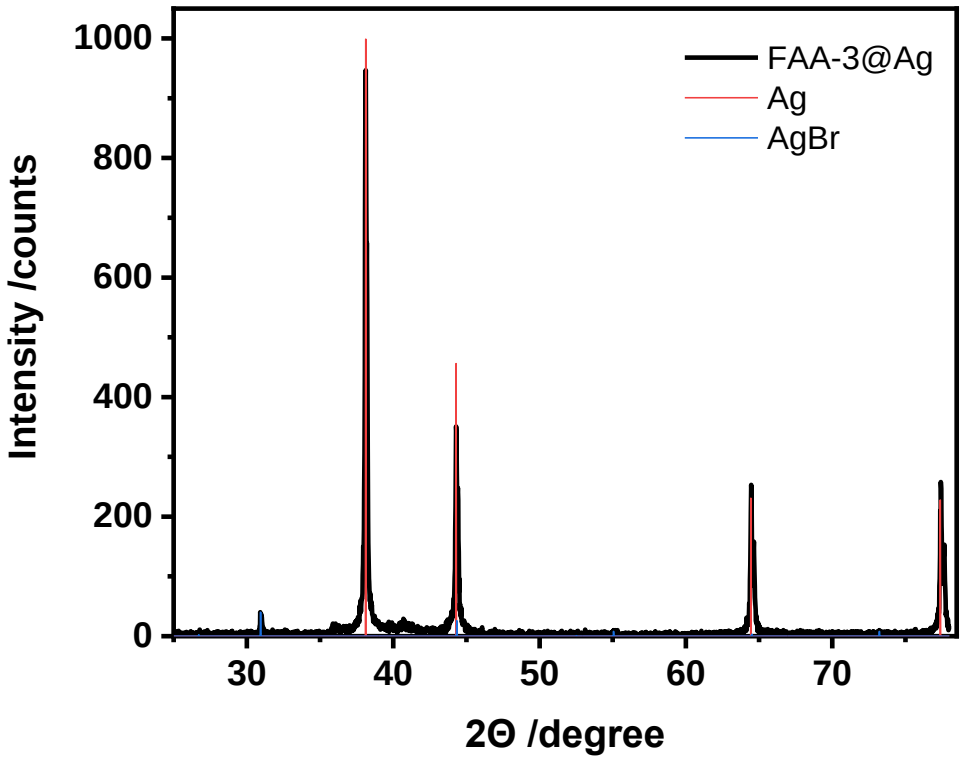

Figure 2. XRD pattern of FAA-3@Ag composite powder compared to silver and silver bromide.

The FAA-3 loading in the composite was determined by thermogravimetric analysis (TGA) measurements (**Error! Reference source not found.**a) and was found to be 8.3 wt%. **Error! Reference source not found.** summarizes other characteristics of the composite - low density (compared to Ag), high polymer vol% and low Ag at%. The experimental values of the density in **Error! Reference source not found.** were also estimated theoretically from equations S1, S2 and S3. The compatibility between the measured and estimated densities also proves that the estimation of the vol% is good.

Table 1. Parameters of the FAA-3@Ag composite

Ionomer wt%	Ionomer vol%	Ag atomic%	ρ_{meas} [g mL^{-1}]	ρ_{est} [g mL^{-1}]

8.3	38.7	45.2	6.5	7.1

In addition to the determination of the polymer loading in the composite, direct proof of the entrapment was achieved by TGA as shown in Figure 3a. Specifically, the derivative profiles in **Error! Reference source not found.**b provide evidence of the effect of entrapped FAA-3 on the decomposition behavior of the composite. It is seen that the main degradation peak is down-shifted by 120 °C, from 540 °C to 420 °C, which is due to the well-known catalytic oxidative effect of Ag[18]. The 4 wt% shoulder at the very high temperature range (700-950 °C) is due to inorganic residues, mainly AgBr (**Error!**

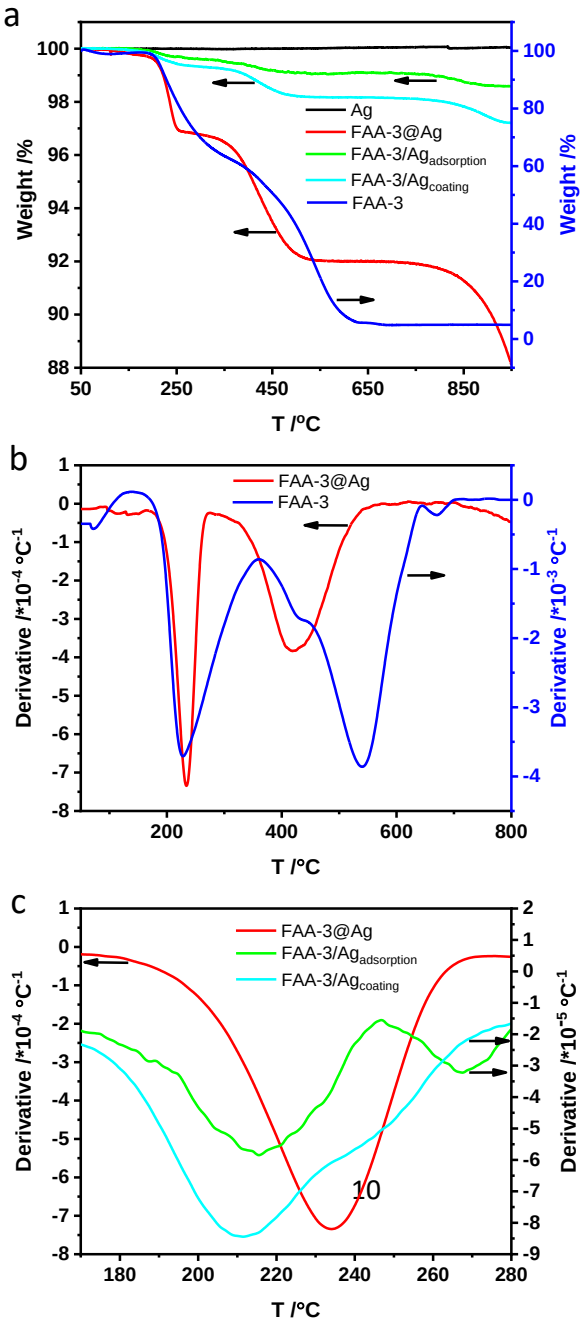

Reference source not found.).

Figure 3: Thermogravimetric analysis (TGA) (a) and differential gravimetric analysis (DTA) (b, c) weight loss profile of FAA-3@Ag (red) compared with pure Ag (black), pure ionomer (blue), ionomer adsorbed on Ag (green) and ionomer coated with Ag (cyan).

The TGA (**Error! Reference source not found.**) also provides additional proof of entrapment by comparing with the weight loss TGA profiles of the pure ionomer, the adsorbed ionomer on the same Ag, and the ionomer-coated Ag. It is seen that when the same amount of ionomer is used for adsorption or for coating, only 1.1 or 1.9 wt%, respectively, are retained, compared with the high loading (8.3 wt%) obtained by entrapment. Moreover, the shift of the second decomposition peak is observed (**Error! Reference source not found.**c): 235 °C for Ag entrapped FAA-3 and 215 °C for adsorbed and coated polymer. By analogy with poly(phenylene oxide) (PPO) and quaternary ammonium-functionalized PPO[46–48] decomposition (PPO backbone decomposes at *t* ~500 °C whereas the functional groups decompose at *t* ~200 °C), we concluded that the decomposition of the functional groups – but not of the backbone - is affected by entrapment and not by adsorption due to the more intimate contact of the functional groups with the metal matrix in entrapped ionomer. The backbone decomposition, which is catalyzed by the presence of the Ag, as mentioned above, is influenced similarly in adsorption and entrapment. Comparison of the weight loss profile of the composite (after water washing, **Error! Reference source not found.**a, c) with unwashed product (**Error! Reference source not found.**) shows identical features, which proves even further that all of the ionomer is entrapped in the Ag matrix.

Yet another key indication of the inherent difference between entrapment and adsorption comes from extended X-ray absorption fine structure (EXAFS) spectrum analysis, which clearly shows (Figure S3 and Table S1, supplementary material) that the coordination number (CN) of silver in the doped case is similar – somewhat lower - to that of pure

silver (CN = 10.3 and 10.6, respectively), whereas surface contact only, reduces the CN significantly to CN = 8.6.

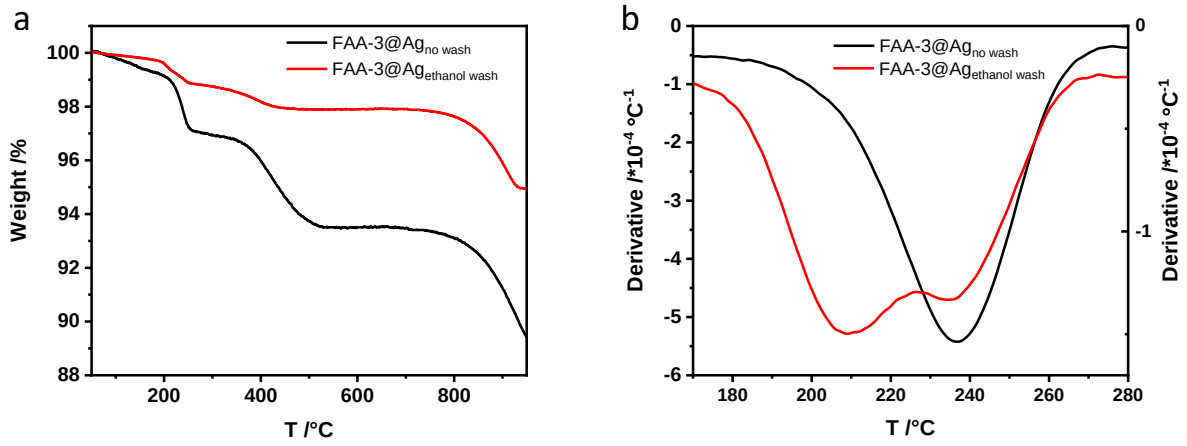

Figure 4: TGA (a) and DTA (b) weight loss profiles of un-washed FAA-3@Ag and ethanol-washed FAA-3@Ag.

The ionomer can be leached out of the composite by washing with ethanol, as can be seen by the decrease in the ionomer amount after washing (**Error! Reference source not found.**a). Part of the washed ionomer is re-adsorbed on the composite, and this is evident from the partial shift of the lower decomposition peak for 235 °C to 215 °C (**Error! Reference source not found.**b).

Focused ion beam (FIB) imaging provides direct visualization of the entrapment of the polymer inside the Ag aggregates (**Error! Reference source not found.**). Voids in the Ag aggregates are clearly seen - from the intra-aggregate 20 nm voids (represented by the small black areas in the grey aggregate in the secondary electrons (SE) image - **Error! Reference source not found.**a, red circles - and by the small white areas in the dark field (DF) image - **Error! Reference source not found.**b, red circles) up to >100 nm, inter-aggregate holes. Additionally, there are areas (**Error! Reference source not found.**d, e), in which the SE image indicates Ag**,** whereas the DF imaging is ambiguously colored – which is indicative of voids in the depth of the silver aggregates. Comparative energy

dispersive spectroscopy (EDS) (**Error! Reference source not found.**c) analysis confirms the presence of the ionomer in those voids - spectrum 2, which measures a void, shows similar Ag content but much higher C content (FAA-3 indicative), compared to spectrum 3, which measures pure Ag area.

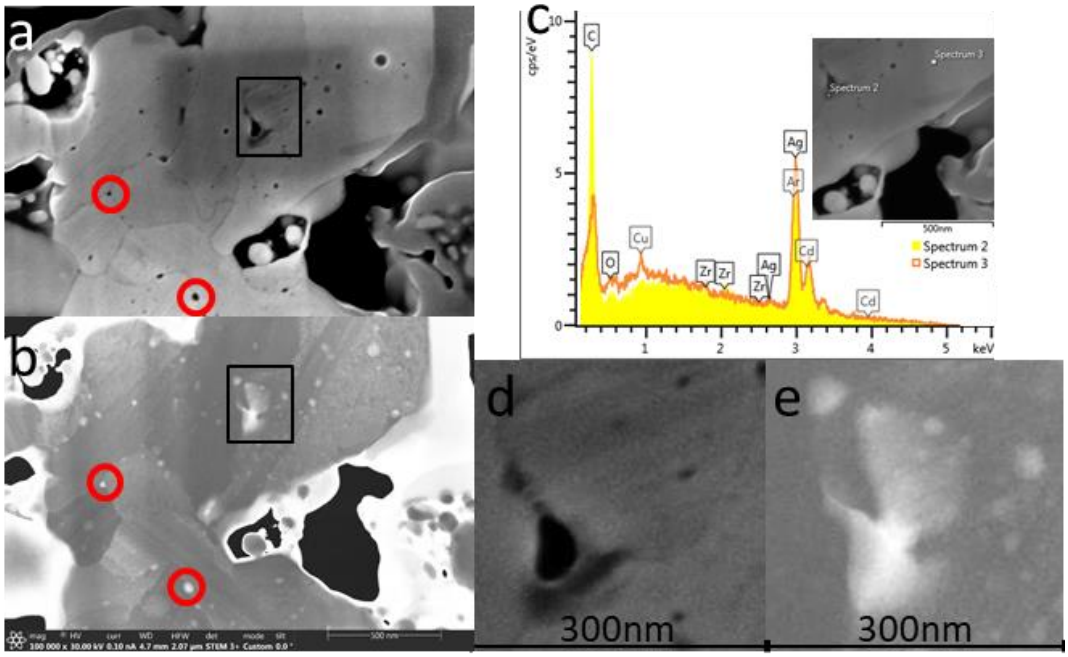

Figure 5: Characterization of the inner parts of FAA-3@Ag aggregate by FIB. Left: STEM images: a – secondary electrons (SE) image (bar: 500 nm); b – dark field (DF) image (bar: 500 nm); c - EDS analysis; d, e - zoom-in of the black rectangular in a,b.

Wavelength dispersive spectroscopy (WDS) analysis (**Error! Reference source not found.**, S4, S5) shows the distribution of the ionomer and the metal in the composite. A good distribution of the ionomer in the silver aggregates is clearly seen. **Error! Reference source not found.**a show that in the as-prepared composite, the ionomer (represented by the pink Br-C areas) is entrapped both by the building blocks and the aggregates. The presence of AgBr (yellow areas) is also seen. Comparison with the

composite in the OH^- form (**Error! Reference source not found.**b) shows that after the ion exchange the only areas with ionomer in the Br^- form (pink areas) are within the silver aggregates, which represent unavailable ionomer sites. Moreover, most of the ionomer (represented by carbon) in the OH^- form of the composite is indeed anion exchanged, as can be seen by the large Ag-C (cyan) areas in the maps. Along with TGA results (**Error! Reference source not found.**a and S2, Supplementary Materials (AgBr)) that show that some of the bromide ions are in AgBr form, leads to the conclusion that the ionomer is entrapped in a Br^-/NO_3^- (from $AgNO_3$) form.

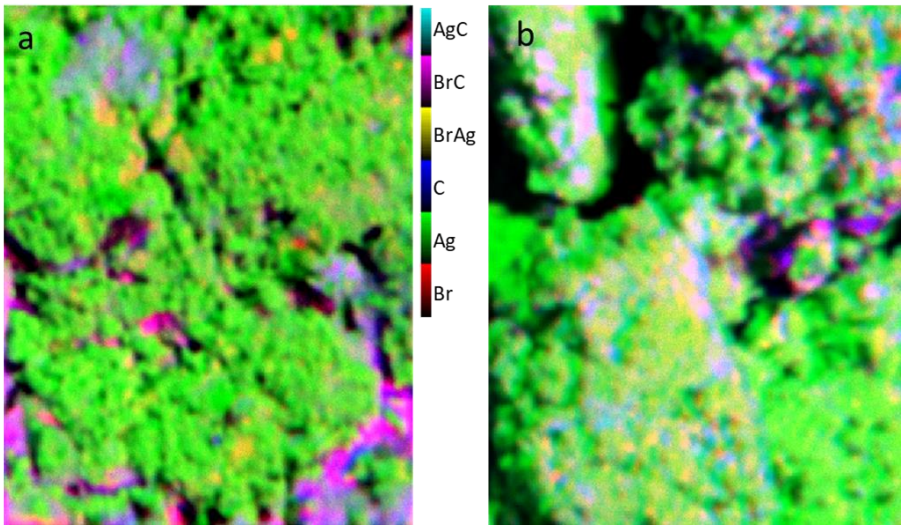

Figure 6. Wavelength dispersive spectroscopy (WDS) elemental mapping of the composite. (a) – FAA-Br^-/NO_3^- form; (b) – FAA-OH^- form. See **Error! Reference source not found.**, **Error! Reference source not found.** for the corresponding separate elemental maps for Br, Ag and C and for SEM image

Ion-exchange measurements

One of the most important parameters of the FAA-3@Ag composite is to retain the ion conducting ability of the ionomer (FAA-3) in its entrapped form. Evaluation of the ionic conductivity of the composite is a major challenge because the ionic mobility[49–51] is 7 orders of magnitude lower than the electronic mobility of metals[52]. Therefore, at first we measured the IEC value, which does not provide direct information regarding the

composite electrode ability to conduct ions through it, but nonetheless gives us sense of the ability of the composite medium to conduct the hydroxide ions. A control ion-exchange experiment was carried out similarly with pure Ag powder.

The IEC values (**Error! Reference source not found.**) of the powder show that the ionomer in the composite retains its hydroxide exchange properties, which means that the entrapped ionomer acts as in its un-entrapped state.

Table 2: Ion-exchange measured parameters (IEC) of the FAA-3@Ag composite.

Composite form	% Exchange	IEC [mmol $g^{-1}_{composite}$]	IEC [mmol $g^{-1}_{ionomer}$]
Powder	92 ± 6	0.18 ± 0.01	2.4 ± 0.1
Pressed pellet	51 ± 6	0.10 ± 0.01	1.3 ± 0.2

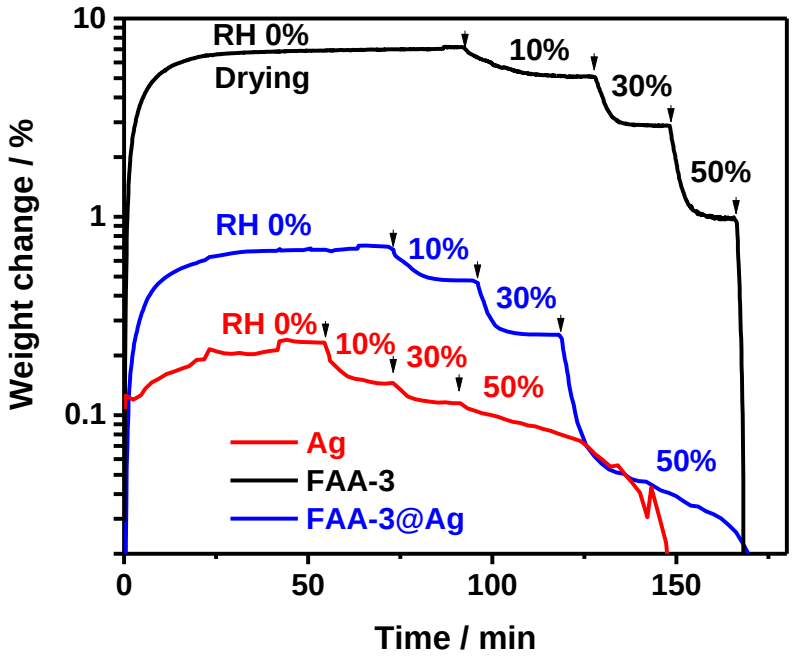

Figure 7. Drying (at relative humidity (RH) 0% and 70 °C) and water uptake (at RH 10, 30 and 50% and 70 °C) curves for pure Ag (red), FAA-3 membrane (black) and FAA-3@Ag composite (blue). Arrows indicate the points of stepwise RH changes.

Table 3. Relative weight changes of pure Ag, FAA-3 membrane and FAA-3@Ag composite during the water uptake measurements.

Parameter	Material			FAA-3@Ag_{calc}[5]/$_{correct}$[6]	WU_{FAA-3}/ $WU_{FAA-3@Ag}$[7]
	Ag	FAA-3	FAA-3@Ag		
WL[1] / %	0.23	7.25	0.71	0.81 / 0.72	10.2
$WU_{10\%}$[2] / %	0.15	5.13	0.48	-	10.7
$WU_{30\%}$[3] / %	0.12	2.87	0.25	-	11.5
$WU_{50\%}$[4] / %	-	0.99	~0.05	-	19.8

[1] Relative weight loss (WL) during drying at RH 0% and the temperature 70 °C.

[2, 3, 4] Water uptake (WU, equation 2) at RH values 10, 30 and 50%, respectively, and the temperature 70 °C.

[5] WL and WU values estimated for FAA-3@Ag composite using the equation $WU(WL) = 0.917 \times WU(WL)_{FAA-3} + 0.083 \times WU(WL)_{Ag}$, where 0.083 is the weight ratio of FAA-3 in the composite (**Error! Reference source not found.**), 0.917 is the weight ratio of Ag in the composite, $WU(WL)_{FAA-3}$ is water uptake (or water loss) value for pure FAA-3 (**Error! Reference source not found.**) and $WU(WL)_{Ag}$ is water uptake (or water loss) value for pure Ag (**Error! Reference source not found.**).

[6] Corrected value of WL using the equation $WL = 0.93 \times WL_{FAA-3} + 0.07 \times WL_{Ag}$, where 0.07 is the weight ratio of FAA-3 in the composite, 0.93 is the weight ratio of Ag in the composite, WL_{FAA-3} is water loss value for pure FAA-3 (**Error! Reference source not found.**) and WL_{Ag} is water loss value for pure Ag (**Error! Reference source not found.**).

[7] Ratio between water uptake values for FAA-3 polymer (WU_{FAA-3}) and for Ag entrapped FAA-3 ($WU_{FAA-3@Ag}$).

Error! Reference source not found. shows relative weight loss and water uptake curves for pure Ag, FAA-3 membrane and FAA-3@Ag composite. Drying at relative humidity (RH) 0% and 70 °C results in relatively low weight changes for pure Ag (0.23%, **Error! Reference source not found.**), whereas FAA-3 membrane loses above 7%, which might be related to the desorption of water molecules. Since the weight of Ag powder undergoes no significant changes, the weight changes of FAA-3@Ag composite can be assigned mainly to the entrapped polymer. The comparison of the calculated weight loss (WL) and water uptake (WU) values (FAA-3@Ag_{calc}, **Error! Reference source not found.**) with the experimentally measured (FAA-3@Ag, **Error! Reference source not found.**) shows that the calculated values exceed the measured ones, indicating that the

actual composition of FAA-3@Ag slightly differs from reported in **Error! Reference source not found.**, containing ~7 wt% of FAA-3, rather than 8.3 wt%. In **Error! Reference source not found.**, it can be seen that the ratio of $WU_{FAA\text{-}3}/WU_{FAA\text{-}3@Ag}$ slightly increases with the RH value. We assume that this observation gives an indirect experimental evidence that the relative amount of the absorbed water vapors on pure polymer is insignificantly but higher than on the entrapped polymer.

AFM - Ionic and electronic conductivity of FAA-3@Ag

To differentiate between electronic and ionic current, two different voltages were applied between the atomic force microscope (AFM) probe and the sample: -0.01 and -0.05 V to determine electronic conductivity of the non-covered Ag at the surface, and -3 V to detect the ionically conductive structure of the ionomer. Additionally, cyclic current-voltage (*I–V*) curves (**Error! Reference source not found.**d) between -4 and +4 V were recorded at different spots (marked in **Error! Reference source not found.**b) to prove the difference between electronic and ionic conductivity of the specific areas of the FAA-3@Ag composite. The black areas in **Error! Reference source not found.**a and b show the electronically conductive structure of the surface with low bias at 25 % and 70 % RH at the same position. The *I–V* curves performed at the black areas (curves 3 and 4) cross the point of origin with a steep linear increase, which verifies their Ohmic behavior. With increasing relative humidity, the electronically conductive surface area decreased from 40 % to 30 %, apparently due to the swelling of the ionomer, which then partly covers the Ag particles. At a sample bias of -3.0 V, low conductivity areas appeared in addition to the highly conductive silver particles (see **Error! Reference source not found.**c). The current values of those areas were approximately one order of magnitude lower and were assigned to ionic faradaic current. The two *I–V* measured at the ionomer phase (curves 1 and 2) demonstrate an electrochemical redox behavior. The *I–V* curve recorded at spot 5 exhibits a mixture of ionic and Ohmic properties.

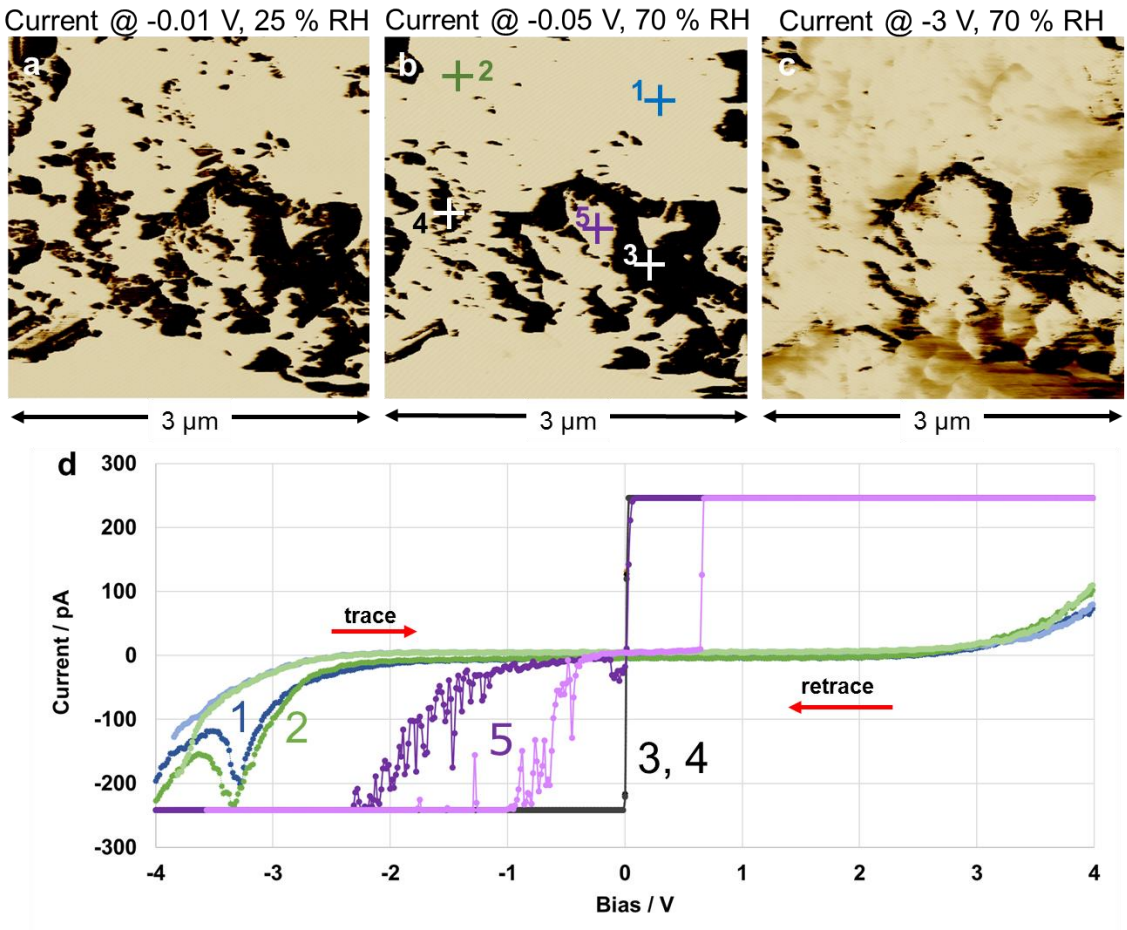

Figure 8: Conductive structure of the surface measured by conductive AFM. Dark colors are related to high conductivity. Current image at -0.01 V and 25 % RH (a), current at -0.05 V and 70 % RH (b), current at -3 V and 70 % RH (c), *I-V*-curves (d) taken at the spots 1-5. Current range of all images: 15 to -100 pA.

Catalytic activity measurements

Error! Reference source not found.a, b show the cyclic voltammograms (CVs) registered for pure Ag and the FAA-3@Ag composite, respectively, in 1 M KOH at 60 °C. Two anodic peaks (A_1 and A_2) appear on the CVs of both materials, whereas cathode scans differ: besides the main peak C_1, a small shoulder C_2 shows up in the Ag-polymer composite. The CVs are similar to those reported for Ag/C catalysts[53] and for polycrystalline silver rods[54]. However, the CVs in **Error! Reference source not found.**a, b are different from the curves on Ag/C[55], Ag nanowires[56], single crystals Ag(111) and

Ag(100)[57] which show three consecutive A_1, A_2 and A_3 peaks. According to the literature,[55,56,57] A_1 (C_2) and A_2 (C_1) correspond to Ag_2O formation (reduction) via Ag oxidation to AgOH (A_1) and then to Ag_2O (A_2). Comparison between the first three CVs (**Error! Reference source not found.**) reveals that after the first cycle the current of peak A_1 increases, and A_2 decreases, totally disappearing in FAA-3@Ag. The C_1 peak currents were decreasing continuously with repetitive cycling for the polymer-Ag composite, whereas for pure Ag the C_1 peak stabilizes and changes little.

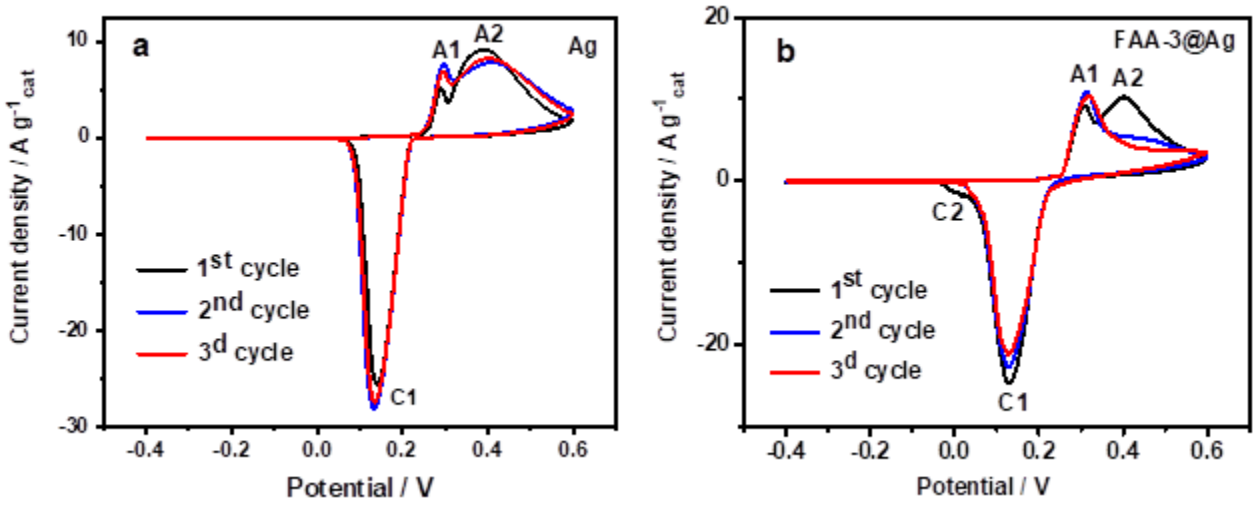

Figure 9: Cyclic voltamograms for pure Ag catalyst (a). Cyclic voltammograms for FAA-3@Ag composite (b). Floating gas diffusion electrode (GDE) method. 1 M KOH, 60 °C, Ar, loadings vary from 0.8 to 1.5 mg_{Ag} cm^{-2} for different GDE, sweep rate 20 mV s^{-1}.

Table 4. Comparison of electrochemical parameters of pure Ag and FAA-3@Ag

Catalyst	Mass activity / A g^{-1}_{Ag}		Tafel slope / mV $decade^{-1}$
	E = -0.05 V	*E* = -0.2 V	
Ag	0.37	7.8	77
FAA-3@Ag	0.42	5.3	107

Error! Reference source not found. presents the comparison of the mass activity in the oxygen reduction reaction (ORR) for pure Ag catalyst and FAA-3@Ag composite. The mass activity (0.42 A g^{-1}_{Ag}) of the composite material are slightly

higher for low overpotential η region (E = -0.05 V) than that for unmodified Ag (0.37 A g^{-1}_{Ag}). In the high overpotential range, an adverse situation is observed, with higher activity on the pure Ag. The Tafel slope on Ag is 77 mV $decade^{-1}$ (**Error! Reference source not found.** S6, **Error! Reference source not found.**), which is slightly lower that reported in the literature[58], while the value is significantly higher for the composite material (107 mV $decade^{-1}$). Most likely, the ORR kinetic hindrance on FAA-3@Ag surface, as well as the lower surface area compared to the pure Ag surface, arises due to the FAA-3[45,59].

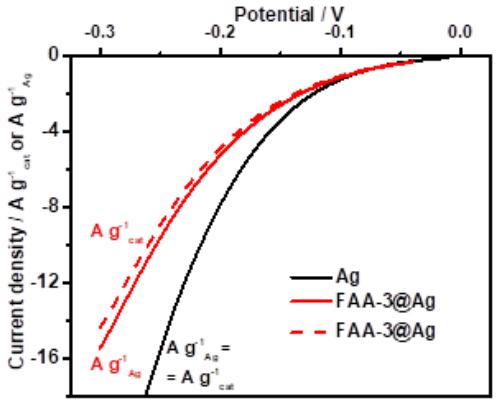

Figure 10. Oxygen reduction reaction (ORR) curves for pure Ag catalyst and FAA-3@Ag composite. Floating GDE method. 1 M KOH, 60 °C, H_2 (flow rate 300 ml min^{-1}), loadings vary from 0.8 to 1.5 mg_{Ag} cm^{-2} for different GDE, sweep rate 1 mV s^{-1}.

Anion-exchange membrane fuel cell (AEMFC) tests

Error! Reference source not found. shows the voltage-current and power density-current curves for AEMFC using Ag (black) and FAA-3@Ag (red) electrocatalysts on the cathode.

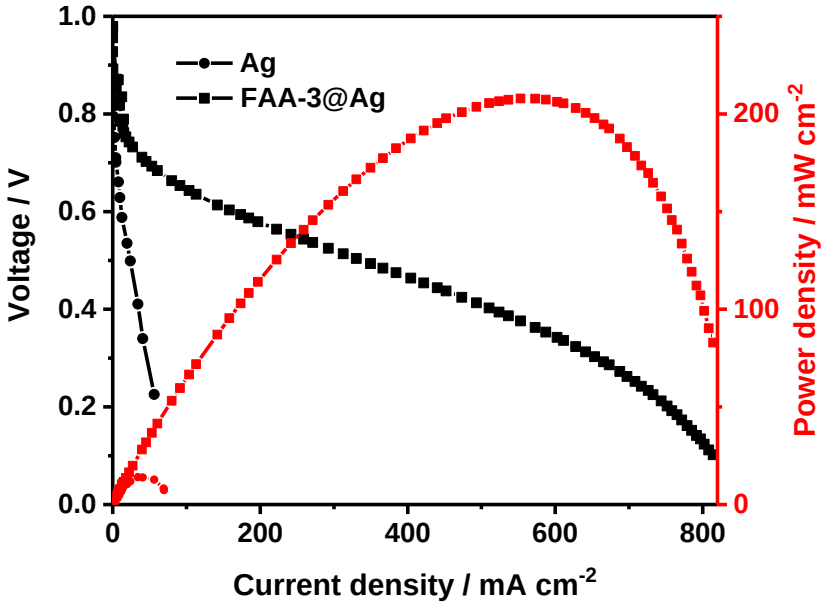

Figure 11. Current-voltage and current-power density curves for H_2-O_2 AEMFC. Membrane electrode assembly (MEA) surface area 5 cm^2. Cell temperature 80 °C. Membrane LDPE-g-poly(-VBTMA+Cl-). Anode: PtRu/Vulcan XC-72R HiSPEC 10000 (40 wt% Pt, 20 wt% Ru); AEI:catalyst ratio 20:80; loading 0.6 mg_{PrRu} cm^{-2}; H_2 and O_2 pressure 1 atm abs., dew point 79 °C. Cathode; Ag (circle) or FAA-3@Ag (square); no additional ionomer; loading 4.5 mg_{Ag} cm^{-2}.

The AEMFC performance with FAA-3@Ag composite is significantly higher than that with pure Ag catalyst. The use of the ionomer entrapped Ag allows reaching peak power density value of ~200 mW cm^{-2} which is more than one order of magnitude higher compared to the peak power density obtained with the pure Ag cathode (~12 mW cm^{-2}). Similarly, with the cell made from FAA-3@Ag catalyst the limiting current is ~800 mA cm^{-2}, one order of magnitude higher than the limiting current of the Ag reference cell (~70 mA cm^{-2}). These results clearly show the advantage of the ionomer@catalyst over the standard catalyst.

Conclusions

In this work we present a new type of composite material that combines both electrocatalytic and ionic properties, by doping silver metal catalyst with anion conducting ionomer at molecular level. We show the entrapment of FAA-3 anion conducting ionomer into the metallic structure of silver catalyst. Characterization of the ionomer doped silver showed that the entrapment can be achieved at molecular level, imparting in that way ionic conductivity to the catalyst. Both catalytic properties and ionic properties were characterized by electrochemical methods and conductive AFM technique, respectively. Electrochemical characterization done by in-situ testing of the composite material as electrode in anion exchange membrane fuel cells, clearly show a significant improvement in cell performance for the ionomer doped silver, as compared to the undoped silver prepared by same synthetic method.

We believe that this new type of synthesis may be expanded to other ionomeric materials and other metal electrocatalysts. As proven here with the FAA-3@Ag system, we believe that this new type of synthesis will impart new unique properties to the metallic-based composite electrocatalysts due to the strong interaction between the metal and the ionomeric entrapped component, imparting ionic conductivity properties to the metal electrocatalyst composite. The significance of this study is anchored in our ability to impart electronic conducting electrocatalysts with ionic conductivity properties. Such materials may have endless applications in several other electrochemistry devices, besides fuel cells that were here first demonstrated.

Acknowledgments: This work was partially funded by the Nancy & Stephan Grand Technion Energy Program (GTEP); by the European Union's Horizon 2020 research and innovation program [grant No. 721065]; by the Ministry of Science, Technology & Space of Israel through the M.Era-NET Transnational Call 2015, NEXTGAME project [grant No. 3-12940], through the Israel-Germany Batteries Collaboration Call 2017 [German grant No. 2675], and through grant No. 3-12948; by the Israel Science Foundation (ISF) [grant No. 1481/17]; by the Israeli Committee of High Education and the Israeli Prime Minister office via the INREP project; by the Russell Berrie Nanotechnology Institute, Technion; by the Israel Innovation Authority through the KAMIN program [grant No.

60503]; by the Ministry of National Infrastructure, Energy and Water Resources of Israel [grant No. 3-13671], and within the framework of the UConn-Technion Energy Collaboration initiative, supported by the Satell Family Foundation, the Maurice G. Gamze Endowed Fund (at the American Technion Society), Larry Pitt and Phillis Meloff, the Eileen and Jerry Lieberman UConn/Israel Global Partnership Fund and the Grand Technion Energy Program (GTEP). GSG also acknowledges support from the Gruenbaum chair in Materials Engineering. The authors acknowledge the Diamond Light Source (project SP18835) for provision of beamtime on the B18 beamline, and Giannantonio Cibin and Barak Menagen for assistance in performing the EXAFS measurements.

Author contributions: Conceptualization, N.R., M.M-L., G.S.G., D.A. and D.R.D.; Methodology, N.R., M.M-L., G.S.G., D.A. and D.R.D.; Investigation, N.R., M.M-L., E.S.D, U.A, R.G., M.H., E.M., J.H., P.C., and A.B.; Resources, R.H., W.M., G.S.G., D.A., and D.R.D.; Writing – Original Draft, N.R., M.M-L. and E.S.D.; Writing – Review & Editing, N.R., M.M-L., E.S.D., G.S.G., D.A. and D.R.D.; Supervision, G.S.G., D.A. and D.R.D.

Declaration of interests: The authors declare no competing interests.

References

1 D. Avnir, *Acc. Chem. Res.*, 2014, **47**, 579–592.

2 D. Avnir, *Adv. Mater.*, 2018, 1706804.

3 L. Chen, I. Polishchuk, E. Weber, A. N. Fitch and B. Pokroy, *Cryst. Growth Des.*, 2016, **16**, 2972–2978.

4 V. B. Kumar, Y. Koltypin, A. Gedanken and Z. Porat, *J. Mater. Chem. A*, 2014, **2**, 1309–1317.

5 M.-A. Neouze and M. Litschauer, *J. Phys. Chem. B*, 2008, **112**, 16721–16725.

6 T. Yutthalekha, C. Wattanakit, V. Lapeyre, S. Nokbin, C. Warakulwit, J. Limtrakul and A. Kuhn, *Nat. Commun.*, 2016, **7**, 12678.

7 H. Yang, D. Chi, Q. Sun, W. Sun, H. Wang and J. Lu, *Chem. Commun.*, 2014, **50**, 8868–8870.

8 H.-P. Yang, Y.-N. Yue, Q.-L. Sun, Q. Feng, H. Wang and J.-X. Lu, *Chem. Commun.*, 2015, **51**, 12216–12219.

9 H.-P. Yang, S. Qin, H. Wang and J.-X. Lu, *Green Chem.*, 2015, **17**, 5144–5148.

10 H.-P. Yang, Q. Fen, H. Wang and J.-X. Lu, *Electrochem. commun.*, 2016, **71**, 38–42.

11 H.-P. Yang, Y.-N. Yue, S. Qin, H. Wang and J.-X. Lu, *Green Chem.*, 2016, **18**, 3216–3220.

12 H.-P. Yang, S. Qin, Y.-N. Yue, L. Liu, H. Wang and J.-X. Lu, *Catal. Sci. Technol.*, 2016, **6**, 6490–6494.

13 M.-A. Neouze and M. Litschauer, *Aust. J. Chem.*, 2008, **61**, 329.

14 G. Palmisano, V. Augugliaro, R. Ciriminna and M. Pagliaro, *Can. J. Chem.*, 2009, **87**, 673–677.

15 Y. Ben-Efraim and D. Avnir, *J. Mater. Chem.*, , DOI:10.1039/c2jm34032a.

16 J. He, L. Iagher, L. Etgar and D. Avnir, *Chem. Commun.*, 2018, **54**, 7203–7206.

17 Y. Aouat, G. Marom and D. Avnir, *Eur. J. Inorg. Chem.*, 2016, **2016**, 1488–1496.

18 H. Behar-Levy, G. E. Shter, G. S. Grader and D. Avnir, *Chem. Mater.*, 2004, **16**, 3197–3202.

19 G. Nesher, G. Marom and D. Avnir, *Chem. Mater.*, 2008, **20**, 4425–4432.

20 L. Shapiro and D. Avnir, *ChemCatChem*, 2013, **5**, 2195–2198.

21 H. Behar-Levy and D. Avnir, *Adv. Funct. Mater.*, 2005, **15**, 1141–1146.

22 B. Britton and S. Holdcroft, *J. Electrochem. Soc.*, 2016, **163**, F353–F358.

23 J. Fan, S. Willdorf-Cohen, E. M. Schibli, Z. Paula, W. Li, T. J. G. Skalski, A.

Tersakian Sergeenko, A. Hohenadel, T. J. Peckham, B. Britton, J. Ward, B. J. Frisken, E. Magliocca, W. E. Mustain, C. E. Diesendruck, D. R. Dekel and S. Holdcroft, *Nat. Commun.*

24 H. Erikson, A. Sarapuu and K. Tammeveski, *ChemElectroChem*, , DOI:10.1002/celc.201800913.

25 Y. Zheng, U. Ash, R. P. Pandey, A. G. Ozioko, J. Ponce-González, M. Handl, T. Weissbach, J. R. Varcoe, S. Holdcroft, M. W. Liberatore, R. Hiesgen and D. R. Dekel, *Macromolecules*, 2018, **51**, 3264–3278.

26 M. R. Hibbs, M. A. Hickner, T. M. Alam, S. K. McIntyre, C. H. Fujimoto and C. J. Cornelius, *Chem. Mater.*, 2008, **20**, 2566–2573.

27 R. C. T. Slade and J. R. Varcoe, *Solid State Ionics*, 2005, **176**, 585–597.

28 Y. S. Li, T. S. Zhao and W. W. Yang, *Int. J. Hydrogen Energy*, 2010, **35**, 5656–5665.

29 G. V. Shteinberg, A. V. Dribinsky, I. A. Kukushkina, L. N. Mokorousov and V. S. Bagotzky, *J. Electroanal. Chem. Interfacial Electrochem.*, 1984, **180**, 619–637.

30 E. S. Davydova, I. N. Atamanyuk, A. S. Ilyukhin, E. I. Shkolnikov and A. Z. Zhuk, *J. Power Sources*, 2016, **306**, 329–336.

31 M. Alesker, M. Page, M. Shviro, Y. Paska, G. Gershinsky, D. R. Dekel and D. Zitoun, *J. Power Sources*, 2016, **304**, 332–339.

32 H. A. Miller, A. Lavacchi, F. Vizza, M. Marelli, F. Di Benedetto, F. D'Acapito, Y. Paska, M. Page and D. R. Dekel, *Angew. Chemie Int. Ed.*, 2016, **55**, 6004–6007.

33 H. A. Miller, F. Vizza, M. Marelli, A. Zadick, L. Dubau, M. Chatenet, S. Geiger, S. Cherevko, H. Doan, R. K. Pavlicek, S. Mukerjee and D. R. Dekel, *Nano Energy*, 2017, **33**, 293–305.

34 M. Bellini, H. A. Miller, M. Pagliaro, F. Vizza, A. Lenarda, P. Fornasiero, M. Marelli, C. Evangelisti, Q. Jia, S. Mukrejee, J. Jankovic, L. Wang, J. R. Varcoe, C. Sharma, I. Grinberg, E. Davydova and D. R. Dekel, *Energy Environ. Sci.*

35 L. Wang, J. J. Brink, Y. Liu, A. M. Herring, J. Ponce-Gonzá Lez, D. K. Whelligan

and J. R. Varcoe, *Energy Environ. Sci*, 2017, **10**, 2154–2167.

36 U. Krewer, C. Weinzierl, N. Ziv and D. R. Dekel, *Electrochim. Acta*, 2018, **263**, 433–446.

37 N. Ziv, W. E. Mustain and D. R. Dekel, *ChemSusChem*, 2018, **11**, 1136–1150.

38 N. Ziv and D. R. Dekel, *Electrochem. commun.*, 2018, **88**, 109–113.

39 N. Ziv, A. N. Mondal, T. Weissbach, S. Holdcroft and D. R. Dekel, *Macromolecules*.

40 Y. Zhou, Q. Lu, Z. Zhuang, G. S. Hutchings, S. Kattel, Y. Yan, J. G. Chen, J. Q. Xiao and F. Jiao, *Adv. Energy Mater.*, 2015, **5**, 1500149.

41 P. Kanninen, M. Borghei, O. Sorsa, E. Pohjalainen, E. I. Kauppinen, V. Ruiz and T. Kallio, *Appl. Catal. B Environ.*, 2014, **156**–**157**, 341–349.

42 D. R. Dekel, *J. Power Sources*, 2018, **375**, 158–169.

43 D. R. Dekel, S. Willdorf, U. Ash, M. Amar, S. Pusara, S. Dhara, S. Srebnik and C. E. Diesendruck, *J. Power Sources*, 2018, **375**, 351–360.

44 B. Bauer, Anion-Exchange Membranes with Improved Stability for Energy Applications, http://www.ias.surrey.ac.uk/workshops/membranes/papers/Bauer.pdf, (accessed 23 October 2018).

45 M. Carmo, G. Doubek, R. C. Sekol, M. Linardi and A. D. Taylor, *J. Power Sources*, 2013, **230**, 169–175.

46 K. H. Gopi, S. G. Peera, S. D. Bhat, P. Sridhar and S. Pitchumani, *Int. J. Hydrogen Energy*, 2014, **39**, 2659–2668.

47 T. Xu, Z. Liu, Y. Li and W. Yang, *J. Memb. Sci.*, 2008, **320**, 232–239.

48 S. Willdorf-Cohen, A. N. Mondal, D. R. Dekel and C. E. Diesendruck, *J. Mater. Chem. A*, , DOI:10.1039/C8TA05785K.

49 J. R. Varcoe, P. Atanassov, D. R. Dekel, A. M. Herring, M. A. Hickner, P. A. Kohl, A. R. Kucernak, W. E. Mustain, K. Nijmeijer, K. Scott, T. Xu and L.

Zhuang, *Energy Environ. Sci.*, 2014, **7**, 3135–3191.

50 A. Amel, N. Gavish, L. Zhu, D. R. Dekel, M. A. Hickner and Y. Ein-Eli, *J. Memb. Sci.*, 2016, **514**, 125–134.

51 A. Amel, S. B. Smedley, D. R. Dekel, M. A. Hickner and Y. Ein-Eli, *J. Electrochem. Soc.*, 2015, **162**, F1047–F1055.

52 V. Palenskis, *World J. Condens. Matter Phys.*, 2013, **03**, 73–81.

53 M. A. Hernández-Rodríguez, M. C. Goya, M. C. Arévalo, J. L. Rodríguez and E. Pastor, *Int. J. Hydrogen Energy*, 2016, **41**, 19789–19798.

54 G. S. Popkirov, M. Burmeister and R. N. Schindler, *J. Electroanal. Chem.*, 1995, **380**, 249–254.

55 S. Maheswari, P. Sridhar and S. Pitchumani, *Electrocatalysis*, 2012, **3**, 13–21.

56 Z.-A. Hu, Y.-X. Wang, Y.-L. Xie, Y.-Y. Yang, Z.-Y. Zhang and H.-Y. Wu, *J. Appl. Electrochem.*, 2010, **40**, 341–344.

57 B. . Jovic, V. . Jovic and G. . Stafford, *Electrochem. commun.*, 1999, **1**, 247–251.

58 X. Ge, A. Sumboja, D. Wuu, T. An, B. Li, F. W. T. Goh, T. S. A. Hor, Y. Zong and Z. Liu, *ACS Catal.*, 2015, **5**, 4643–4667.

59 A. Orfanidi, P. Madkikar, H. A. El-Sayed, G. S. Harzer, T. Kratky and H. A. Gasteiger, *J. Electrochem. Soc.*, 2017, **164**, 418–426.